Geophysical Prospecting

EAGE EUROPEAN ASSOCIATION OF GEOSCIENTISTS & ENGINEERS

Geophysical Prospecting, 2014, **62**, 1–16 doi: 10.1111/1365-2478.12066

Interferometric interpolation of sparse marine data

Sherif M. Hanafy[1,2]* and Gerard T. Schuster[1]

[1]*King Abdullah University of Science and Technology (KAUST), PSE Division, Thuwal 23955-6900, Saudi Arabia and* [2]*Geophysics Dept. Faculty of Science, Cairo University, Giza, Egypt*

Received August 2011, revision accepted January 2013

ABSTRACT

We present the theory and numerical results for interferometrically interpolating 2D and 3D marine surface seismic profiles data. For the interpolation of seismic data we use the combination of a recorded Green's function and a model-based Green's function for a water-layer model. Synthetic (2D and 3D) and field (2D) results show that the seismic data with sparse receiver intervals can be accurately interpolated to smaller intervals using multiples in the data. An up- and downgoing separation of both recorded and model-based Green's functions can help in minimizing artefacts in a virtual shot gather. If the up- and downgoing separation is not possible, noticeable artefacts will be generated in the virtual shot gather. As a partial remedy we iteratively use a non-stationary 1D multi-channel matching filter with the interpolated data. Results suggest that a sparse marine seismic survey can yield more information about reflectors if traces are interpolated by interferometry. Comparing our results to those of f-k interpolation shows that the synthetic example gives comparable results while the field example shows better interpolation quality for the interferometric method.

Key words: Interferometric, Upgoing, Downgoing, Interpolation.

INTRODUCTION

Typical marine surface seismic profiles (SSP) are ideally designed for a regular recording grid but in practice suffer from irregularities in recording geometry, coarse receiver spacing and narrow recording apertures, especially in the cross-line direction. The result can be inadequate subsurface illumination and distortions in the migrated image.

Trace interpolation can sometimes be used to overcome the sparse sampling of traces. To address this problem different interpolation methods have been proposed such as the generalized interpolation method (Gulunay 2003) and the frequency-wavenumber interpolation method (Zwartjes and Sacchi 2007). For accurate results, Gulunay (2003) assumed the dip content of lower frequencies is the same as dip content of original frequencies and that events are linear in the input records, while Zwartjes and Sacchi (2007) assumed that the shot gather consists in a limited number of planar events. Naghizadeh and Innanen (2011) interpolated traces in the frequency domain using a generalized Fourier transform to identify the space-wavenumber evolution of non-stationary spatial signals at each temporal frequency.

Other methods (van Dedem and Verschuur 2005; Abma and Kabir 2006) use certain assumptions to fill in the missing traces in marine data e.g., the data have a sparse representation in a certain domain, or rely on existing information such as the seismic velocity distribution (Baumstein *et al.* 2005). In most cases, they do not use the redundant information available in free-surface multiples.

The previously mentioned methods use the total recorded field to fill in receiver gaps and missing traces. However, successful cases of imaging downgoing multiples have been demonstrated with VSP data (Jiang, Yu and Schuster 2005) and ocean-bottom seismic (OBS) data (Grion *et al.* 2007). Another example is Muijs, Robertsson and Holliger (2007) who applied a 2D deconvolution imaging condition to both primaries and multiples. For comparison between different interpolation methods, Abma and Kabir (2005) showed the differences between 7 interpolation methods applied to 3 synthetic models.

*E-mail: sherif.geo@gmail.com

Multiples are often considered as noise and, therefore, are removed from data. This point of view ignores the benefit that multiples provide either redundant or new information about the reflectivity distribution. For example, Berkhout and Verschuur (2006), Curry and Shan (2006, 2010), and Ramirez, Hokstad and Otnes (2007) used multiples to interpolate for missing traces in a seismic survey. In Berkhout and Verschuur (2006), two steps are required for trace interpolation; 1) an inverse focal transformation is obtained to separate primaries from multiples and 2) the separated multiples are transformed to primaries and used to fill in the gaps. Ramirez *et al.* (2007) interpolated and extrapolated missing traces by interferometry, where direct waves and free-surface ghosts are cross correlated with measured field traces to estimate the missing traces. Their method requires the recording of both pressure and its normal derivative. If the normal derivative data are not available, two approximations are made: (1) the medium at the surface is assumed to be homogeneous and (2) the local angle between the ray approximation of the wavefield and the vector normal to the surface is assumed to be zero. Curry and Shan (2010) interpolated only near-offset traces by creating a pseudoprimary and error prediction filter (EPF); in the 3D case it is limited with a poor spatial distribution of sources. Groenestijn and Verschuur (2009a,b) used sparse inversion to estimate only the primaries and only for near-offset traces. Another interferometry interpolation method was presented by Wang, Luo and Schuster (2009) who correlated seismic traces to fill in the gaps of near-offset traces in a marine experiment. Artefacts associated with the far-field assumption were partly removed by a matching filter.

In this paper we show how to interpolate marine seismic data by interferometry using a model-based Green's function (Dong and Schuster 2008; Wang *et al.* 2009). This method transforms surface and sea-bed related multiples into primaries recorded at virtual receivers[1] both inside and outside the receiver array; no assumptions and no velocity model for the deeper layers are needed, however the thickness of the water and the seismic wave velocity in the water are required; in addition a rough estimate of the seismic wave velocity of the layer below the water bottom is desired. The interpolated data can be used for migration, velocity analysis and tomography. Multiples can also be used to illuminate much wider areas of the subsurface and remove the generated artefacts by the Wang *et al.* (2009) approach.

[1] A virtual receiver point is a non-physical receiver at the position of a modelled source, where we generate a virtual trace by redatuming actual traces recorded at a distance to the position of the virtual trace.

This paper is organized into 4 parts: 1) introduction, 2) theory section that presents the reciprocity equations for a two-state system and shows how it can be used for interpolation, 3) numerical tests for both synthetic and field data and 4) conclusions.

THEORY

Sheng (2001) suggested that interferometric imaging of seismic data can be used to reduce problems with poor seismic illumination of the subsurface due to limited recording geometry; the key idea is that free-surface multiples can be used to extend the subsurface illumination. Following this, Wang *et al.* (2009) developed and applied an interferometric interpolation method to seismic data. In their method, the surface-related multiples are used to predict missing traces in gaps, where sparse data can also be interpolated using an SSP $\rightarrow$ SSP transform (Wang *et al.* 2009). In contrast, our method uses a hybrid interferometric method where both the model-based and data-based Green's functions are used to interpolate the data. This procedure was originally introduced by Dong and Schuster (2008) and later applied to 2D data by Wang *et al.* (2009). The advantage of the hybrid approach over a purely data-based method is that sources and receivers can be located anywhere for the model-based Green's function as long as the topography of the sea floor is known. The model-based Green's function is for a two-layer model and a band-limited point source, as shown in Fig. 1. The diagrams show how seismic traces (with both sources and receivers below the free surface) are correlated with sparsely distributed seismic traces to generate a dense distribution of seismic traces. This correlation operation is required by the acoustic reciprocity equation of correlation type for a two-state system (Appendix A), where one state is the acoustic field associated with the multi-layered model shown in Fig. 1(b) and the other state is associated with the sea-floor model shown in Fig. 1(a). Since the source and the physical and virtual receivers are not in the stationary-phase zone we integrate along the receiver locations (Snieder, Wapenaar and Larner 2006; Ramirez and Weglein 2009).

The reciprocity equation of correlation type (Schuster 2009 and Appendix A) for the geometry of Fig. 1 can be described as:

$$G(\mathbf{B}|\mathbf{A}) - G_0(\mathbf{A}|\mathbf{B})^* = \int_{S_s} [G_0(\mathbf{x}|\mathbf{B})^* \frac{\partial G(\mathbf{x}|\mathbf{A})}{\partial n_x} - G(\mathbf{x}|\mathbf{A}) \frac{\partial G_0(\mathbf{x}|\mathbf{B})^*}{\partial n_x}] d^2x, \quad (1)$$

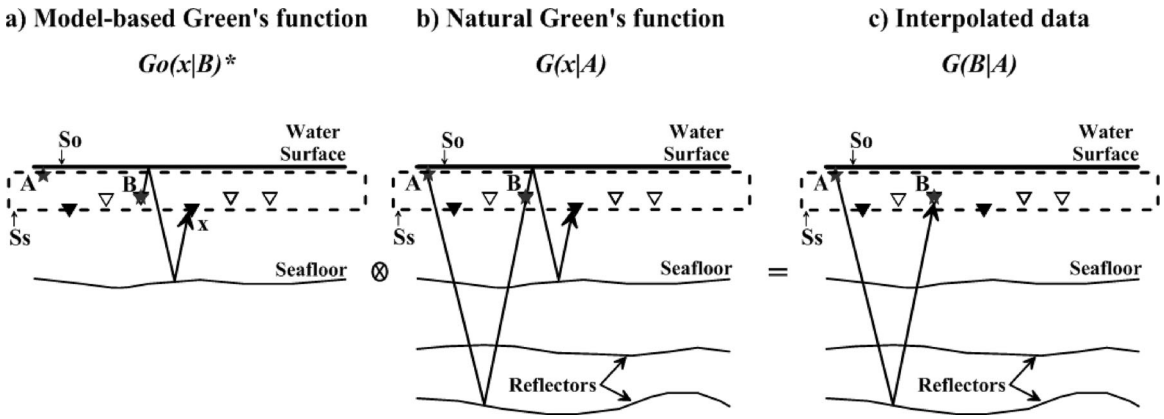

Figure 1 Ray diagrams showing the interpolation process. Here, the white triangles indicate the locations of virtual receivers where traces are created from the original data recorded at the black triangle positions. Both $G(\mathbf{x}|\mathbf{A})$ and $G_0(\mathbf{x}|\mathbf{B})$ can be data-based Green's functions, but in this case $G_0(\mathbf{x}|\mathbf{B})$ is computed for the two-layer sea-water model. **A**, **B** and **x** are the source point, virtual receiver point and true receiver point, respectively, S_o is the free surface and S_S is the integration boundary.

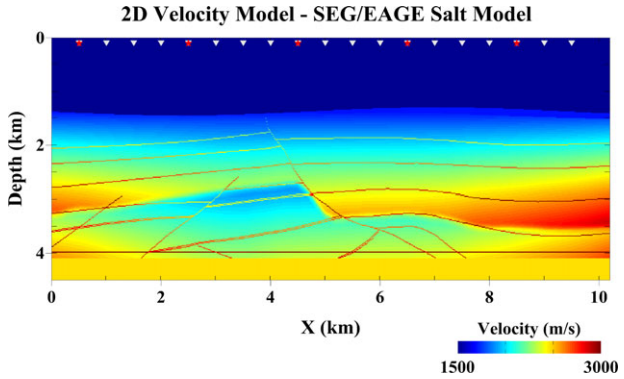

Figure 2 A cross-section of the SEG/EAGE salt model used for the 2D interpolation test. The sea floor is at about 1400 m. The white triangles represent receiver points and the red stars represent shot points. In this test we generated 141 shot gathers with an interval of 50 m and each gather has 601 traces with an interval of 5 m.

where $G_0(\mathbf{x}|\mathbf{B})$ is the model-based Green's function for a water-layer model that contains both primaries and high-order multiples and $G(\mathbf{x}|\mathbf{A})$ is the Green's function for the actual earth model in the frequency domain (Dong and Schuster 2008; Hanafy, Cao and Schuster 2009). Here, sources at **A** are just below the free surface, physical receivers at **x** are along the integration surface and virtual shots/receivers at **B** are slightly above the lowered dashed integration surface[2] that is below the source line. Here, **B** represents the shot point location for the model-based shot gathers and the virtual receiver points for the interpolated shot gathers. S_s is the integration surface along the lower dashed boundary and the integration along the free surface vanishes because both Green's functions are zero and the outward pointing $\hat{\mathbf{n}}$ is the unit vector normal to the boundary. The contributions from the vertical boundaries at infinity to the left and to the right will be ignored.

The above equation is a reciprocity equation of correlation type for two different states, which can be used for interpolation or extrapolation of traces. If both pressure field data and particle velocity data are recorded, then equation (1) can be directly used to estimate the interpolated traces. Otherwise the far-field approximation is applied to equation (1) to obtain the far-field approximation (Schuster 2009)

$$G(\mathbf{B}|\mathbf{A}) \approx 2ik \int_{S_s} G(\mathbf{x}|\mathbf{A}) G_0(\mathbf{x}|\mathbf{B})^* dx^2 + G_0(\mathbf{A}|\mathbf{B})^*. \qquad (2)$$

The term $G_0(\mathbf{A}|\mathbf{B})^*$ in equation (2) represents the acausal part of the interferometric data. Using the total field for both $G(\mathbf{x}|\mathbf{A})$ and $G_0(\mathbf{x}|\mathbf{B})^*$ in equation (2) will produce artefacts, however, using only upgoing fields will reduce these artefacts (Wapenaar and Fokkema 2006). To implement this equation, two Green's functions are required; (1) the upgoing portion of the two-layer model-based Green's function $G_0(\mathbf{x}|\mathbf{B})^*$ that only accounts for the point source response of the free-surface and ocean-bottom interfaces. A finite-difference (FD) solution to the 2D acoustic wave equation is used to estimate the model-based Green's function. This FD calculation is possible because the sea-floor topography is well known beneath any exploration survey. (2) The second Green's

[2] To avoid the principal value singularity (Schuster 2009) associated with the direct wave in $\frac{\partial G_0(\mathbf{x}|\mathbf{B})^*}{\partial n_x}$ in equation (1) the virtual receivers **B** should be slightly above the integration surface. In practice we mute the direct waves prior to integration and use only the reflections in $G_0(\mathbf{x}|\mathbf{B})$ and $G(\mathbf{x}|\mathbf{A})$. Thus, the deleterious effects of integration with a near-singular kernel are avoided.

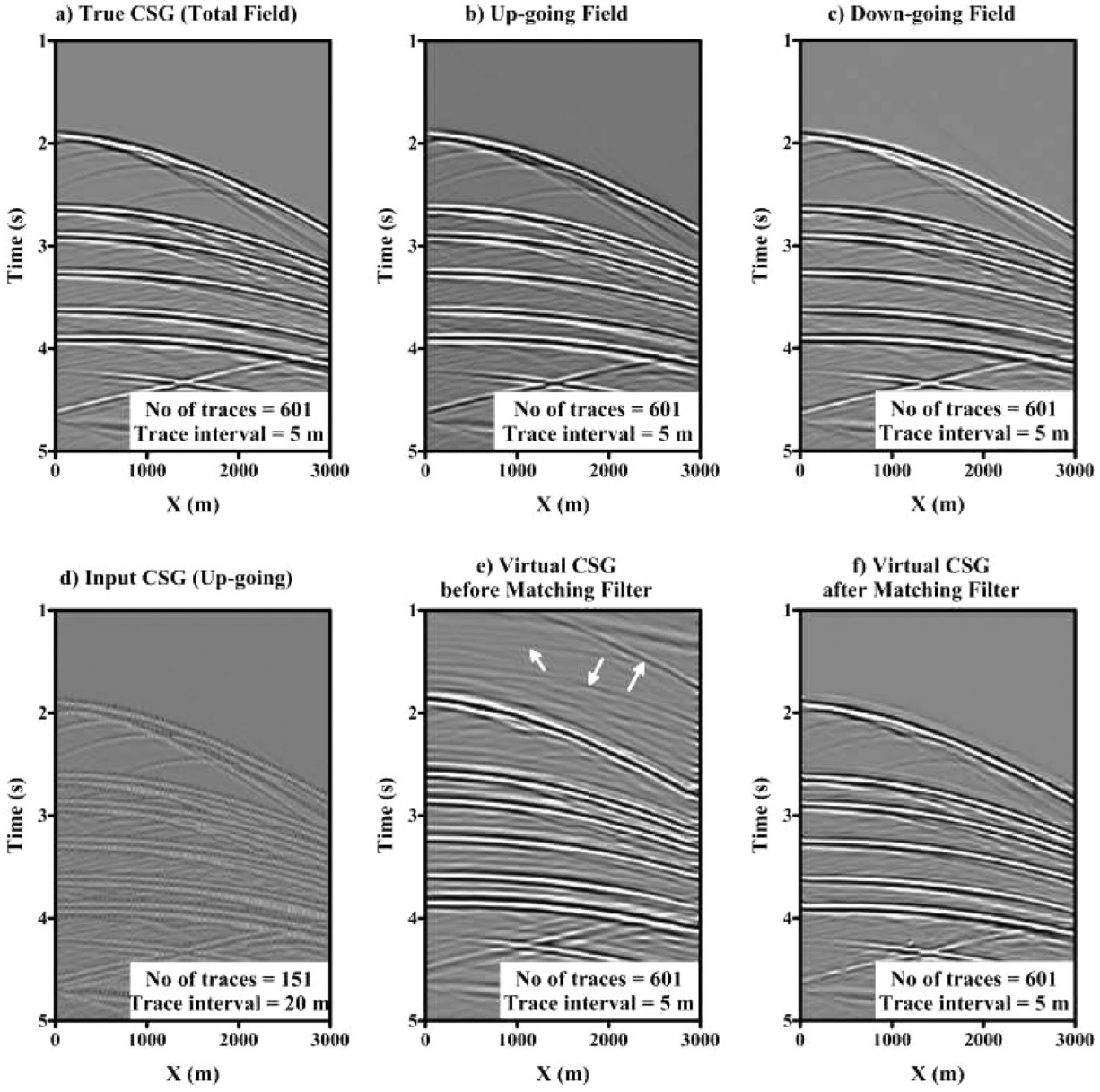

Figure 3 a) The reference shot gather of the seismic survey with a trace interval of 5 m. Here, the estimated minimum wavelength in the x direction is 51 m; b) the upgoing field; c) the downgoing field; d) the sparse shot gather used for the interpolation test, where the trace interval is 20 m; e) the interpolation results before; and f) after using a matching filter. White arrows are referring to some artefacts examples in the virtual shot gather before using the matching filter.

function $G(\mathbf{x}|\mathbf{A})$ accounts for the upgoing portion of the data. The key idea for interpolation is that the free surface acts as a perfectly reflecting mirror so that second and third views, i.e., free-surface related multiples, of the subsurface can be used to fill in the trace gaps, as indicated in Fig. 1.

In practice, it is not always possible to accurately estimate the upgoing portion of $G(\mathbf{x}|\mathbf{A})$ with the consequence that noticeable artefacts can be generated in the interferometric shot gather. In this case, we use the matching filter that will mitigate this problem and reduce the artefacts. Ramirez and Weglein (2009) gave more details regarding the interferometric reconstruction of seismic data using different models with source/receiver points inside or outside the integration volume.

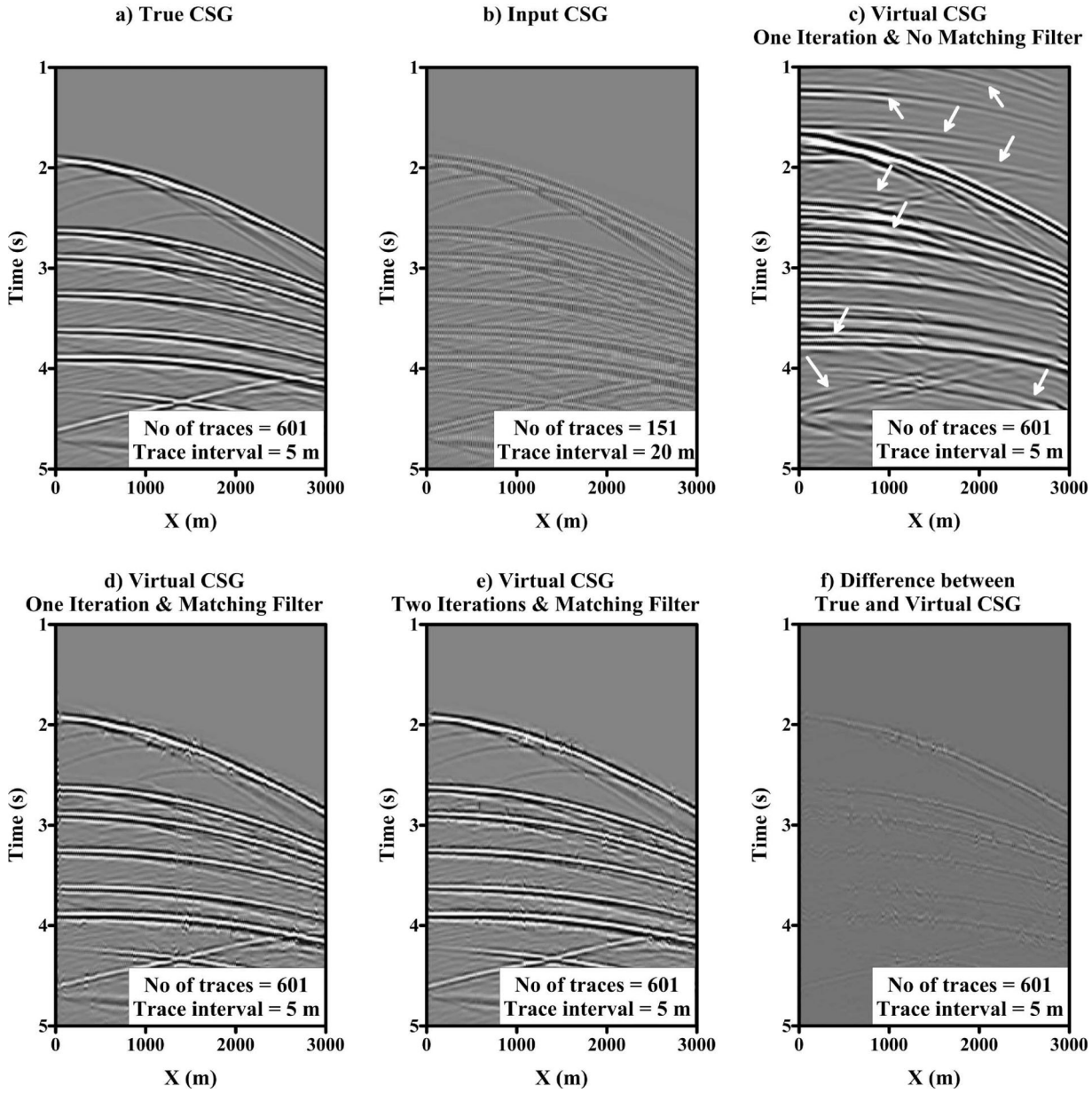

Figure 4 a) The reference shot gather of the seismic survey with a trace interval of 5 m. Here, the estimated minimum wavelength in the x direction is 51 m; b) the sparse shot gather used for the interpolation test, where the trace interval is 20 m; c) the interpolation results before the matching filter, white arrows are referring to some artefacts; d) same virtual shot gather after one iteration of the matching filter, most of the artefacts are removed but the results show some noise; e) the virtual shot gather after repeating the interpolation process twice and the matching filter 4 times, here, the artefacts and noise are highly eliminated; f) the difference between the final virtual shot gather and the true shot gather magnified 2 times for better display.

Matching filter

To mitigate the artefact problem we use a 1D local matching filter (Wang 2003; Verschuur 2006; Aoki 2009; Huo and Wang 2009) to reduce the artefacts and smooth the interpolated traces. A matching filter $f(t)$ in the time domain is defined so that it solves the equation

$$\mathcal{G}^T(\mathbf{B}, t|\mathbf{A}) = \mathcal{G}^V(\mathbf{B}, t|\mathbf{A}) \star f(t), \tag{3}$$

where $\mathcal{G}^T(\mathbf{B}, t|\mathbf{A})$ and $\mathcal{G}^V(\mathbf{B}, t|\mathbf{A})$ denote the sparse true and virtual traces in the time domain, respectively, **A** is the source

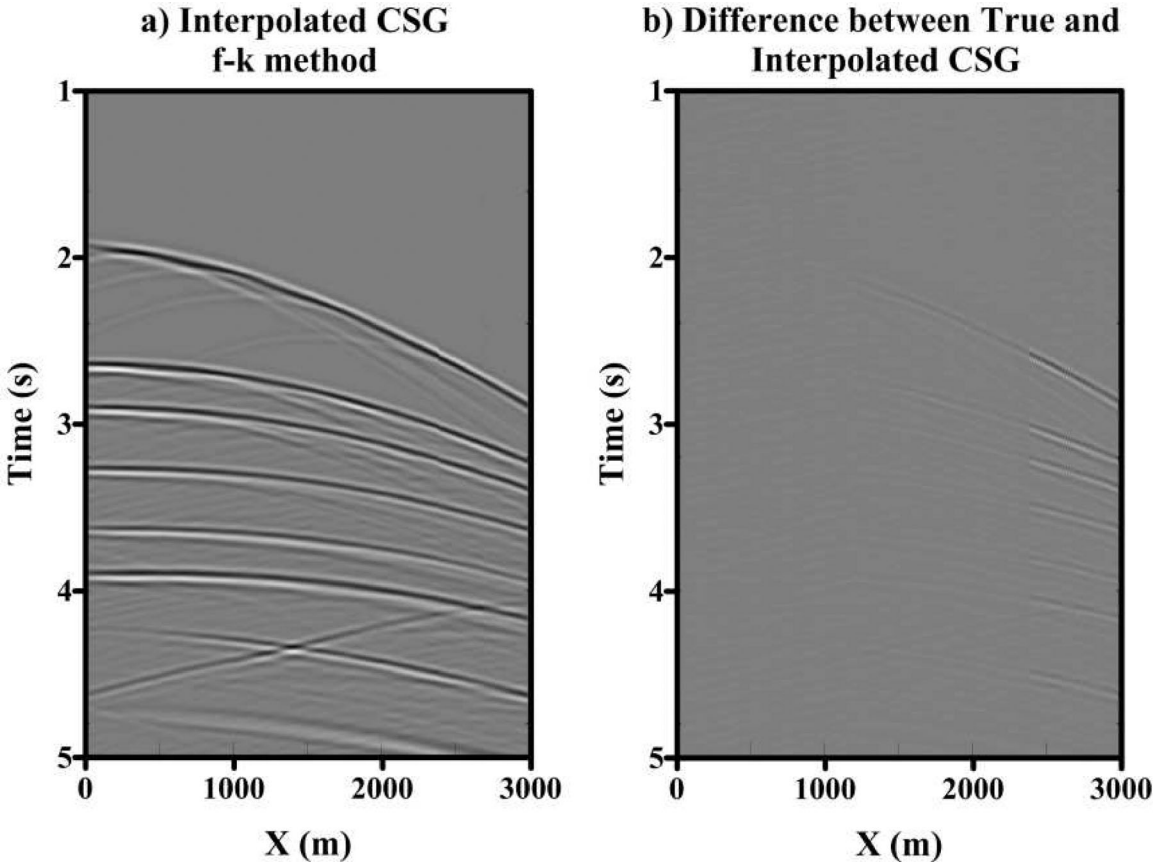

Figure 5 a) The interpolated shot gather using f-k interpolation. The input shot gather is shown in Fig. 4(b). b) The difference between the f-k interpolation results and the true CSG.

location and **B** is the receiver location, $\star$ denotes temporal convolution and $f(t)$ is the required filter. And in the frequency domain equation (3) is given by,

$$G^T(\mathbf{B}|\mathbf{A}) = G^V(\mathbf{B}|\mathbf{A})F, \tag{4}$$

where $G^T(\mathbf{B}|\mathbf{A}) = \mathcal{F}(\mathcal{G}^T(\mathbf{B}, t|\mathbf{A}))$, $F = \mathcal{F}(f(t))$ and $\mathcal{F}$ represents the temporal Fourier transform. The filter F can be found from

$$F = \frac{G^T(\mathbf{B}|\mathbf{A})^* G^V(\mathbf{B}|\mathbf{A})}{[G^V(\mathbf{B}|\mathbf{A})]^2 + \varepsilon}, \tag{5}$$

where ε is a small damping factor. Using equation (5) the filter F that locally matches the virtual traces to the true ones at the sparse receiver locations is found. It is computationally inexpensive because its temporal length is only several periods long in the time direction and several traces in the offset direction.

The optimal matching filter window is selected[3] using a trial-and-error testing procedure on synthetic data and then the filter F is computed by a least-squares solution method. The filter is then applied to all virtual traces that do not have corresponding true traces within the selected window.

The small filter window is incrementally shifted over the virtual shot gather with a 50% overlap in neighbouring windows and the entire filtered virtual gather is reconstructed by summing the results from all of the windows. The matching filter not only corrects for the wavelet of predicted events but also can suppress artefacts (Wang *et al.* 2009). The procedure of cross-correlation and summation of correlated traces followed by the application of a matching filter is iterated (Huo and Wang 2009) in Appendix B.

[3] Typically, the window size is equal to a few traces wide and a few periods long.

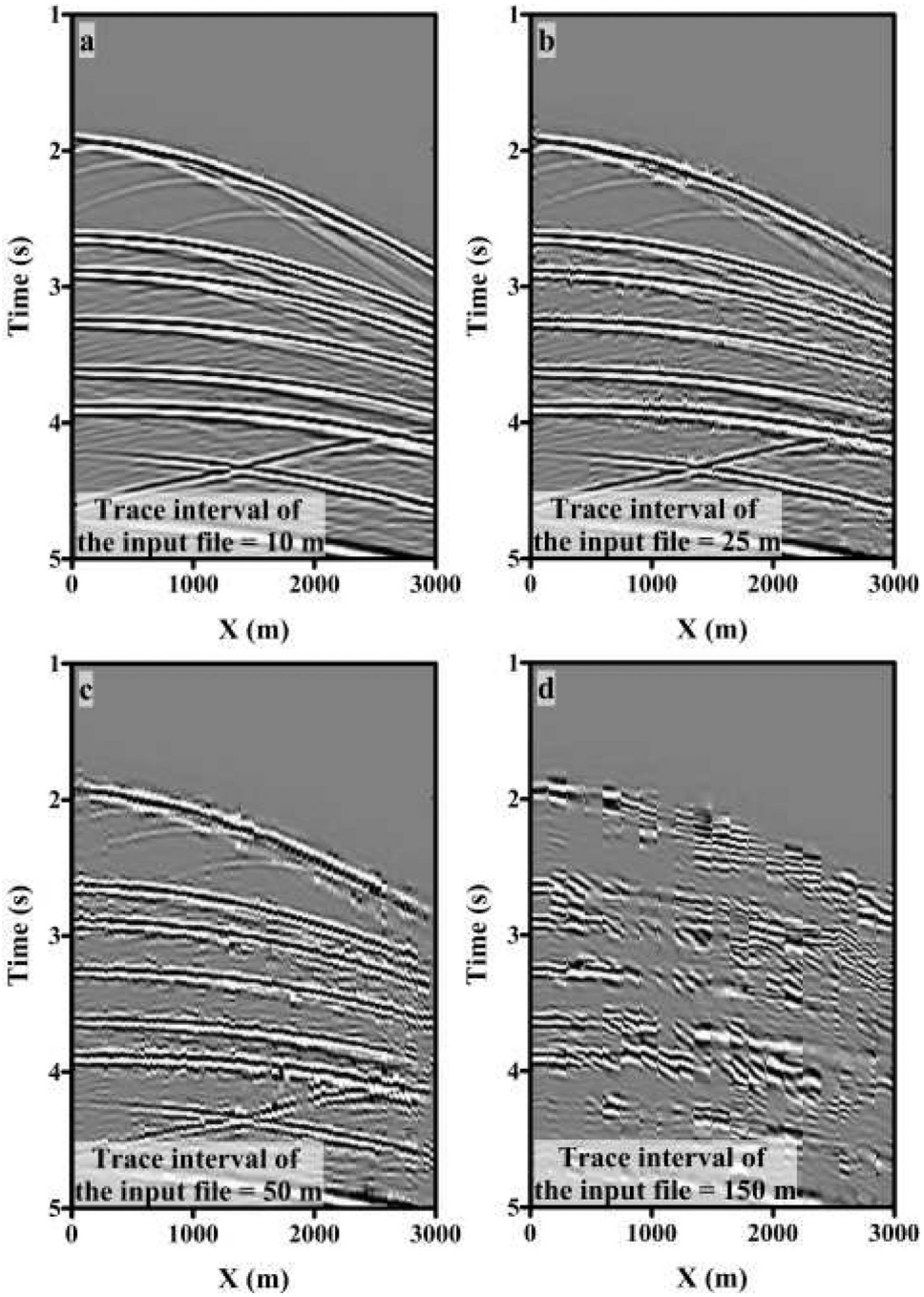

Figure 6 The virtual shot gather for the 2D synthetic example where the trace intervals of the input shot gather are (a) 10 m, (b) 25 m, (c) 50 m, and (d) 150 m.

NUMERICAL TESTS

The proposed interferometric interpolation method is tested on several velocity models. In this work, only the results from the SEG/EAGE velocity model are presented.

2D synthetic example using the upgoing approach

We simulated acoustic data recorded by a 2D seismic marine survey with 2 streamers where one streamer is above the other, the source time history is a Ricker wavelet with a 10 Hz peak

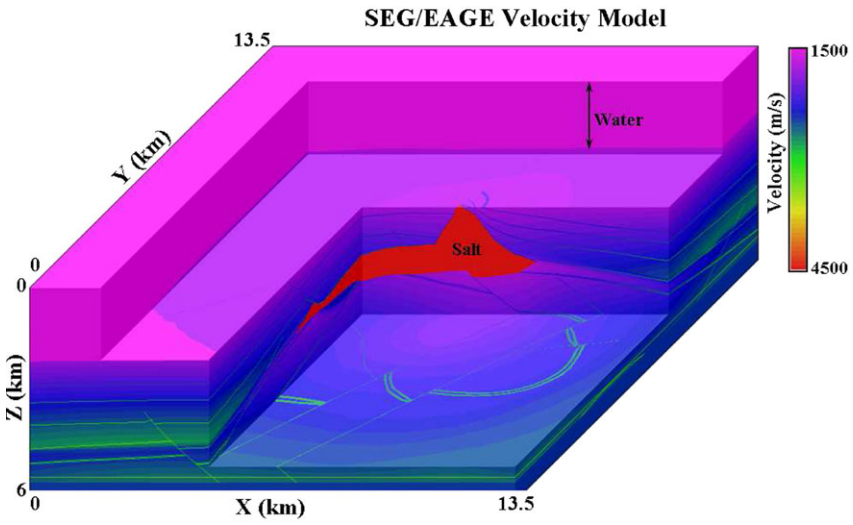

Figure 7 The SEG/EAGE salt model used for the 3D interpolation test. The sea floor is at about 2100 m.

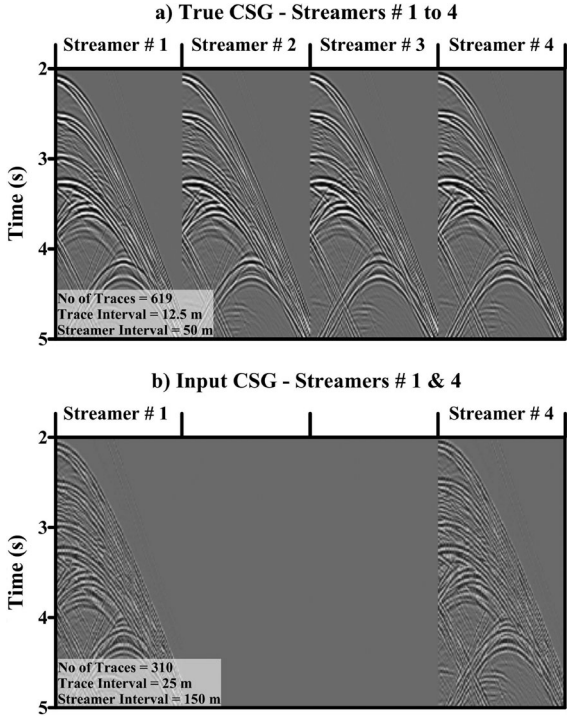

Figure 8 a) Synthetically generated shot gather of streamers 1–4. The generated data consist in 34 cross-lines with 619 receivers per cross-line, the in-line receiver interval is 12.5 m, cross-line spacing of 50 m and the total number of receivers is 21046. b) Shot gather used as input to the interpolation method. The shown traces are associated with the 1^{st} and 4^{th} streamers of the original shot gather. Data are resampled to the in-line receiver interval of 25 m and cross-line streamer interval of 150 m; we kept every 3^{rd} streamer (1, 4, 7, ..., 34) and the other streamers are removed. Here, each streamer consists in 310 receivers and the total number of receivers in the input data is 3,720. We zoomed in -between 2–5 s for better display.

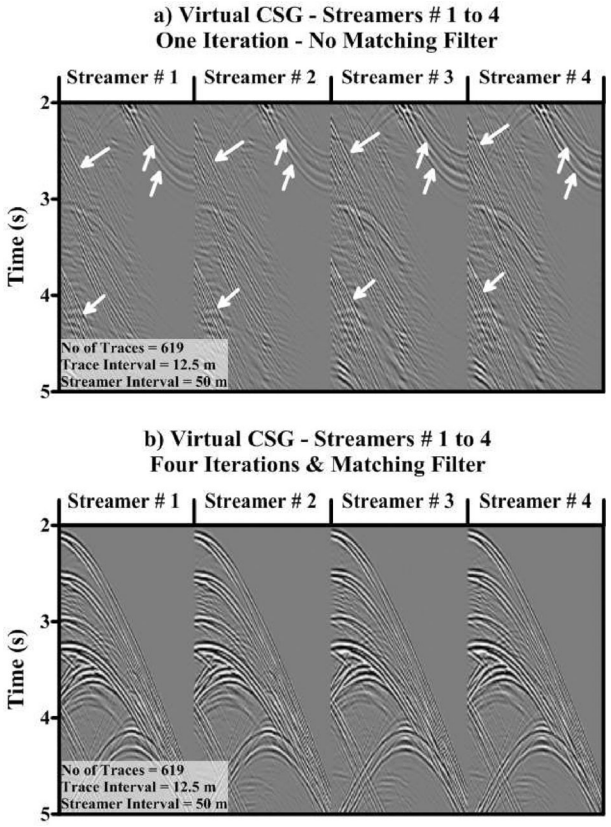

Figure 9 a) The interpolation results of the SEG/EAGE velocity model with one interpolation iteration and no matching filter, where there are many artefacts as shown by the white arrows. This figure shows traces for streamers 1–4. b) The interpolation results after using 4 iterations of interpolation and matching filters. This figure shows streamers 1–4 and zooms in -between 2–5 s for better display.

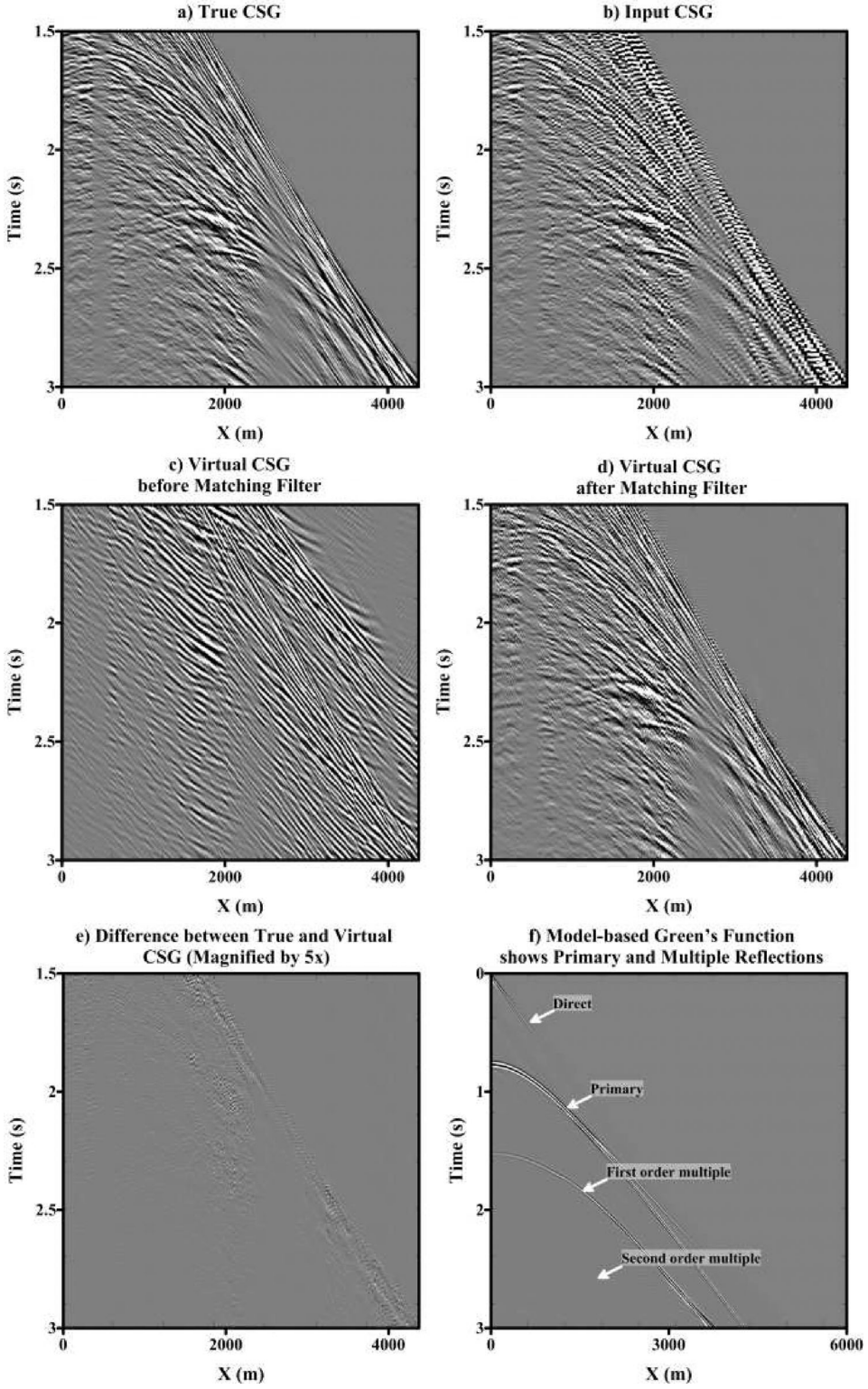

Figure 10 a) The true shot gather of the 2D field survey with a trace interval of 12.5 m. Here, the estimated minimum wavelength in the x direction is 84 m; b) the sparse shot gather used for the interpolation test, where the trace interval is 37.5 m; c) the interpolation results before the matching filter; d) same virtual shot gather after two iterations of the matching filter, most of the artefacts are removed; e) the difference between d and a; and f) a sample shot gather of the model-based Green's function.

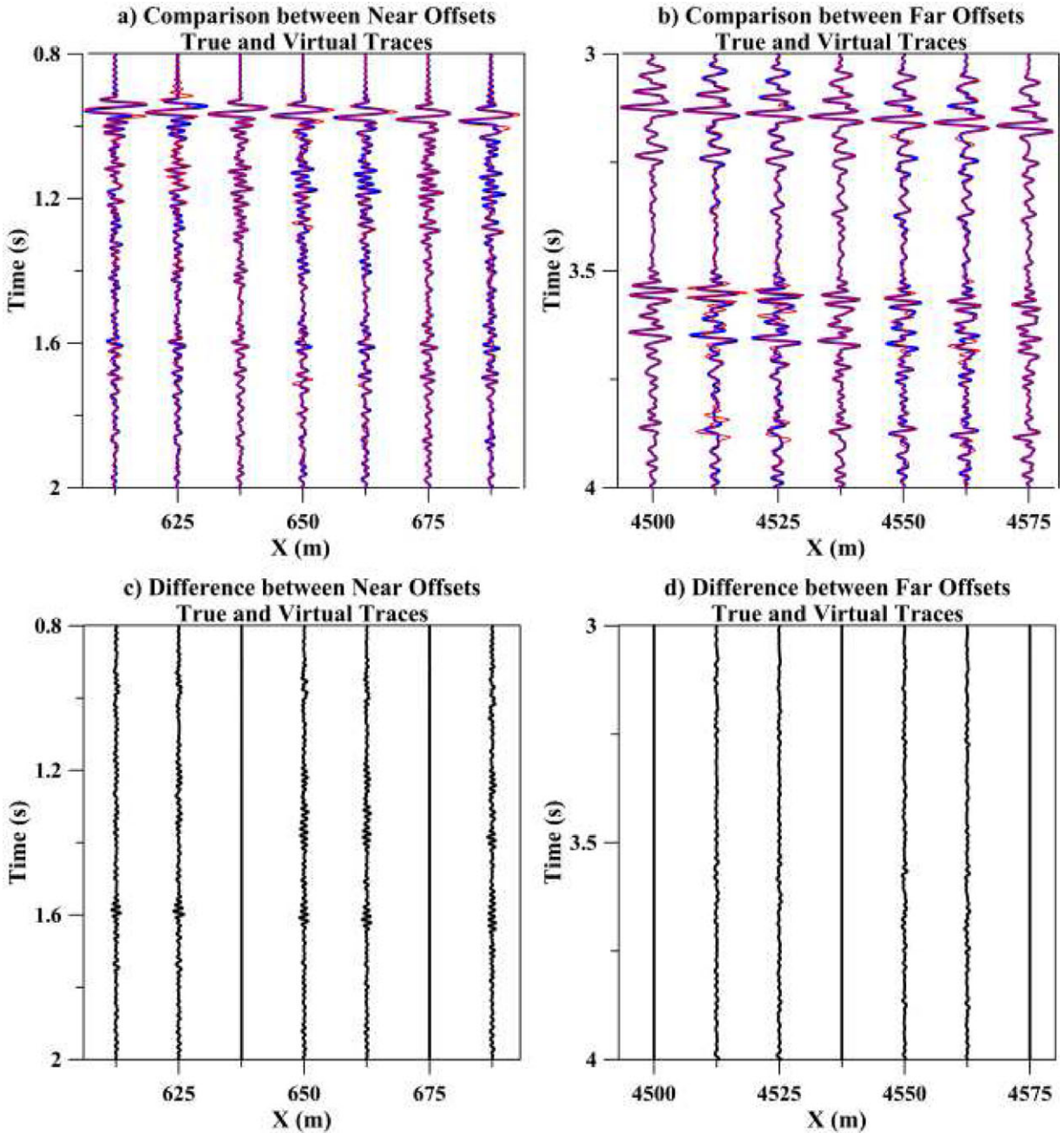

Figure 11 Zoomed in display of the comparison between the reference (blue) and virtual (red) traces; selected traces are at near- (a) and far- (b) offsets. c) and d) show the difference between the traces shown in a) and b).

frequency, each streamer has 601 receivers and the receiver interval is 5 m. The streamer depths are 5 m and 15 m below the water surface for streamers 1 and 2, respectively; and the total recording time is 10 s. Figure 2 shows the 2D velocity model extracted from the SEG/EAGE salt model. We used this velocity model to generate the synthetic shot gather using a finite-difference solution to the 2D acoustic wave equation. Fig. 3(a) shows the upper streamer shot gather after muting the direct waves. The computed data are separated into up- and downgoing pressure fields shown in Figures 3(a,b), respectively. The upgoing field is reassembled into traces with a trace interval of 20 m (Fig. 3d) and the result is used as the

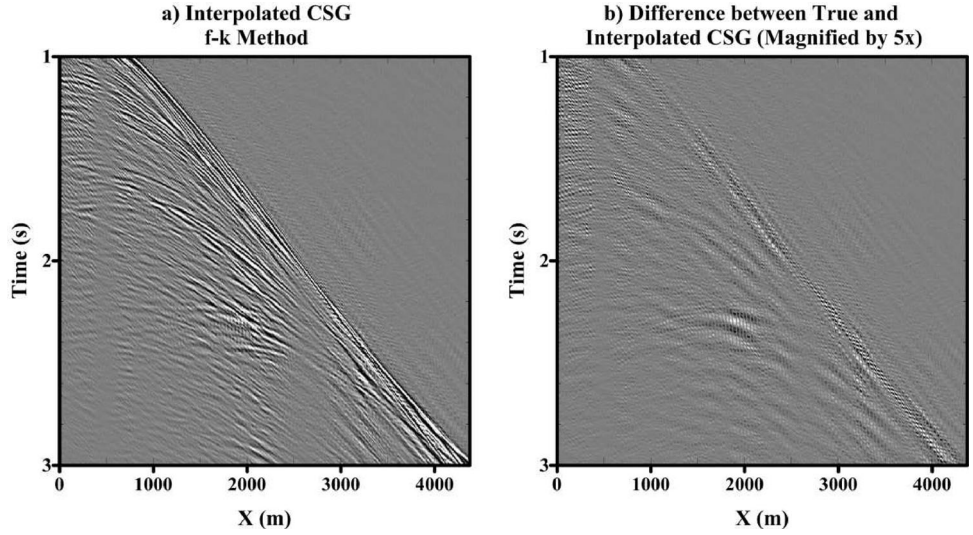

Figure 12 a) The interpolated shot gather using the f-k method, here the input shot gather to the f-k is the same as Fig. 10(a). b) The difference between the true shot gather and the f-k interpolated shot gather. These two figures should be compared to the interferometric interpolation in Figs. 10(d,e).

input shot gather to equation (2). The output virtual shot gather (601 traces at 5 m intervals) is shown in Fig. 3(e). Here, we can see some artefacts caused by the limited recording aperture and the 'ghost' waves. To mitigate the artefacts shown in the virtual shot gather, we used the matching filter with a window length size of 0.16 s long by 3 traces wide, a matching filter length of 0.076 s and the window is shifted by 0.032 s. The results after applying the matching filter are shown in Fig. 3(f). The virtual shot gather (Fig. 3e) and the input shot gather (Fig. 3d) are used to generate the matching filter (equation (5)). Here, the filter in equation (5) is computed by only using the virtual traces $G^V(\mathbf{B}|\mathbf{A})$ and the recorded traces $G^T(\mathbf{B}|\mathbf{A})$ at the sparsely sampled receivers. The virtual shot gather after using the matching filter (Fig. 3f) closely resembles the true shot gather (Fig. 3a).

2D synthetic example using the total field approach

In this test we will assume that up- and downgoing separation is not possible and we will use the total field data as input to equation (2). The total field (Fig. 4a) is resampled at 20 m trace intervals (Fig. 4b) and equation (2) is used to compute the virtual shot gather (Fig. 4c). The calculated virtual shot gather shows more artefacts than the virtual shot gather in Fig. 3(e). This is expected since we use the total field and not the upgoing field. Iteratively applying the matching filter gives the shot gather shown in Fig. 4(d) after 3 iterations. The matching filter parameters for all iterations are the same and are equal to those used in the previous example. The true shot gather (Fig. 4a) closely resembles the virtual shot gather (Fig. 4d) but there is some noise in the virtual shot gather. Repeating the process one more time (i.e., interferometric interpolation and 3 iterations of the matching filter) removes some of the noise (Fig. 4e). Here, we first replace the amplitudes of every virtual trace that shares the same location with a true trace with that trace, then we use that virtual shot gather, which contains true traces and virtual traces from a previous iteration, as the input to the second iteration. Comparison between the final virtual shot gather (Fig. 4e) and the true shot gather (Fig. 4a) shows a better agreement and Fig. 4(f) shows the difference between the final virtual shot gather and the true shot gather magnified 2 times.

Comparing the interpolated traces computed from the upgoing data to those from the total field data (Figs. 3 and 4) shows almost identical results. Using the upgoing field as the input for the interferometric interpolation has three advantages: (1) it produces fewer artefacts, here artefacts are due to the limited aperture of receivers, (2) only one iteration of the matching filter is sufficient in this example to remove the artefacts, and (3) inexpensive calculation time. The disadvantage here is we need to complete the up- and downgoing separation, which, for field data, sometimes is not possible. The advantage of using the total field approach is that the up- and downgoing separation is not required but the disadvantages are increased computational costs and the potential to introduce false information in the virtual traces due to the excess

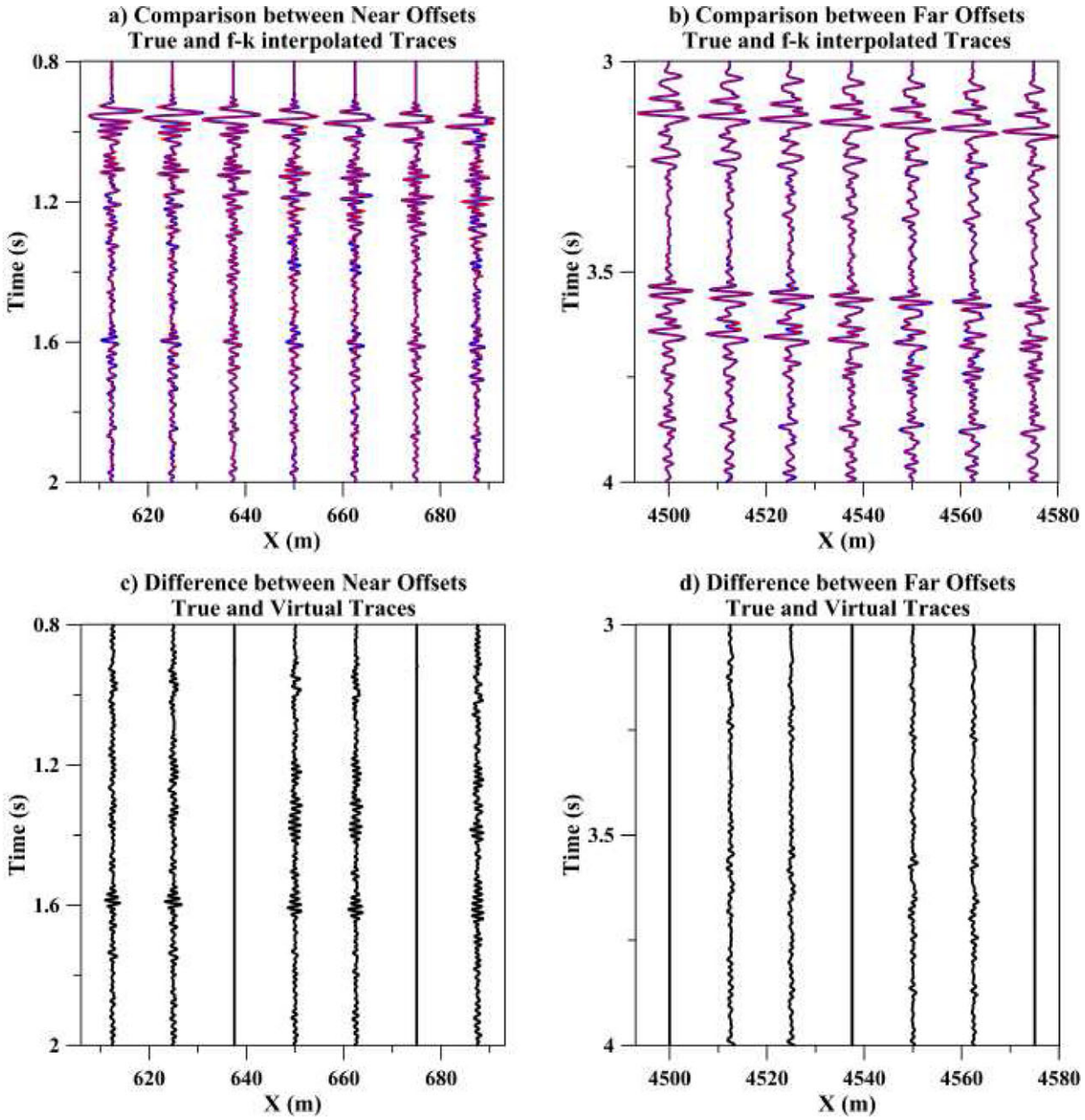

Figure 13 Same as Fig. 11 except f-k interpolation traces are used.

use of the matching filter. This later possibility is obviated by careful testing with synthetic data.

To compare our results to a standard interpolation method, we used a commercial processing package[4] to apply f-k interpolation to the sparse input shot gather (Figs. 4b) to give the interpolated shot gather shown in Fig. 5(a). Comparing the f-k interpolated shot gather to the true shot gather (Figs. 4a) shows a very good agreement, which is

[4] We used the 'f-k interpolation' option in 2D ProMax software from the Landmark package. The input parameters are either double or triple the number of traces and the minimum velocity value; here we chose double the traces and 1500 m/s as the minimum velocity. The software will do the following; (1) the input data are ensambled padded with zeros in time and space; (2) extended data are f-k transformed; (3) apply a low-cut velocity filter using the given minimum velocity value to the extended f-k transformed data; and (4) apply an inverse f-k filter to obtain the interpolated data.

similar to our interferometric interpolation results. Comparing Fig. 4(f) to Fig. 5(b) shows that both figures have the same level of noise at the far-offset traces; the noises in the interferometric interpolation case are due to the lack of enough traces for the summation, while in the case of f-k interpolation they are due to the steep reflection moveout. The near-offset f-k interpolated traces show less noise than the interferometric interpolation approach. The advantage of our method is that the f-k method requires regularly spaced receivers, while our method does not. The disadvantage is that the interferometric method will have more difficulty with land data because the free-surface multiples in land data are not as distinct as in the marine data.

The suggested interpolation methods may break down if the number of input traces is too few or the interval between input traces is too large. Figure 6 shows the output of 4 different input shot gathers with trace intervals of 10, 25, 50 and 150 m. We notice that as the input trace interval increases the quality of the virtual shot gather decreases. This quality degradation will likely increase with increasing complexity of the velocity model and frequency of the source.

3D synthetic example

We used the SEG/EAGE velocity model (Fig. 7) to simulate a narrow azimuth marine survey with 34 streamers, where each streamer is composed of 619 receivers at a 12.5 m receiver interval. The cross-line streamer interval is 50 m, the near-offset hydrophone is at 200 m and the far-offset hydrophone is at 7925 m (Fig. 8a). The synthetic shot gather has 3001 samples/trace at a temporal sample interval of 4 ms, which gives a total time of 12 s and the goal is to resample the synthetic data to a sparse version and then interpolate the traces in both the in-line and cross-line directions. The input version of the synthetic shot gather consists in traces for 12 streamers at a 150 m streamer interval and 310 receivers per streamer at a receiver interval of 25 m (Fig. 8b). Figure 9(a) shows the virtual shot gather (1^{st} to 4^{th} streamers) after one interpolation iteration and before the application of a matching filter. Artefacts due to the interferometry algorithm are shown in the virtual shot gather (Fig. 9a). To minimize these artefacts and improve the final results the following steps are used:

(1) A 1D multi-channel local matching filter is iteratively applied to the interpolated traces to remove the artefacts. The matching filter parameters used for all iterations are the following; window length is 0.16 s long and window width is 3 traces, the matching filter length is 0.076 s and the window is shifted by a time interval of 0.032 s

(2) All virtual traces at the actual trace locations are replaced with the corresponding true traces.

(3) The output of step 2, which contains both the true traces and the generated virtual traces, is used as the new input to interactive interpolation.

(4) Finally, steps 1–3 are repeated several times (4 times in this work) to produce the final virtual shot gather (Fig. 9b). A large improvement in quality between iterations 1 and 2 is expected because in iteration 1 we use only true traces, while in iteration 2 we use both the true and generated virtual traces. Virtual shot gathers will slowly improve after iteration 2 since the updated virtual traces will contain fewer artefacts after each iteration.

Figure 9(b) shows the final virtual shot gather, where the artefacts are largely eliminated. Comparing the final virtual shot gather (Fig. 9b) with the synthetic shot gather (Fig. 8a) shows a very good agreement.

Field data example

A 2D marine data set is used to test the proposed interferometric interpolation method. This data set was recorded in the Gulf of Mexico with 515 shots and 480 traces per shot gather. The receiver spacing is 12.5 m and the total recorded time is 10.24 s with a sample interval of 2 ms and 5120 samples per trace. We tested the proposed interpolation method on one shot gather.

A low-pass filter (60 Hz) is applied to the data (Fig. 10a) and then the first arrival times are picked and used to calculate the water velocity. A finite-difference approximation is used to estimate the model-based Green's functions $G_0(\mathbf{x}|\mathbf{B})^*$ for a model that only contains the free surface and sea-bottom interfaces. The direct waves are muted before interpolation. To minimize artefacts, the data should be separated into up- and downgoing components and only the upgoing components should be used. In this example, we did not have enough information to compute the up- and downgoing separation, so we used the total field for interpolation and used a matching filter to reduce the artefacts.

A sparse distribution of traces (Fig. 10b) is used as input data, where there were only 160 traces per shot gather with a trace interval of 37.5 m Equation (2) is used to interpolate the deleted traces and Fig. 10(c) shows the virtual shot gather before the application of the matching filter. Artefacts are shown in the virtual shot gather (Fig. 10c), so a local matching filter is used to remove them. The window size used for the matching filter is 0.24 s long and is 3 traces wide, the matching filter length is 0.084 s and the window is shifted by a 0.04 s interval.

Fig. 10(d) shows the virtual shot gather after 2 iterations of the matching filter; for each iteration the input traces were the output traces of the previous iteration (Appendix B). A good match between the true and virtual shot gathers is shown in the final result (Fig. 10d). For a more detailed comparison, Fig. 11 displays some traces from the true data and the same traces from the virtual gather at the far- and near-offsets. The high degree of similarity between the true and virtual traces demonstrates the accuracy of the interpolation technique.

Figure 12(a) shows the results using the f-k interpolation method and Fig. 12(b) shows the difference between the f-k interpolated results and the true shot gather, which shows higher noise than our suggested interferometric interpolation approach (Fig. 10e). Figure 13(a,b) shows a trace-to-trace comparison between the true and f-k interpolated traces for near- and far-offsets, respectively. Fig. 13(c,d) shows the differences between the true and f-k interpolated traces. Comparing Figs. 13(c,d) to Fig. 11(c,d) shows that the interferometric interpolation traces have less noise than the f-k interpolation traces.

CONCLUSIONS

We present an interferometric interpolation method based on the far-field approximation to the reciprocity equation of correlation type. Results with both synthetic data (2D and 3D) and field data (2D) show that this method could kinematically interpolate the sparse seismic data to dense distribution receivers. The artefacts from the interferometric interpolation can be partly suppressed by using only the upgoing components of the data but we can avoid this separation step by using the total pressure field combined iteratively with a matching filter. This filter is calibrated by matching the virtual trace with the recorded trace at the actual recording positions and then the matching filter can be applied to the virtual traces that were interpolated to fill the gaps in the original shot gather.

No exact velocity model is required for this approach; however, the thickness of the water layer and the velocity of the seismic waves in the water are required and a rough estimate of the seismic wave velocity of the layer below the water is desired. The interpolated data can be used for migration, velocity analysis and tomography.

The merits of interferometric interpolation are that it is applicable to marine data with irregular acquisition geometries and the virtual primaries generated from the multiples can be stacked onto the original primary reflections, which has the potential to increase the signal-to-noise ratio.

A difficulty with this procedure is that it is not a true amplitude method due to the limited aperture of the data. The truncated aperture in the correlation integral can lead to amplitude errors in the predicted traces, even though the kinematic predictions are accurate. This problem can possibly be alleviated by least squares interferometry. A serious challenge is when the input date are severely aliased, so that the accuracy of the virtual traces is reduced. A partial remedy is to apply an anti-aliasing filter (Cao and Schuster 2010) to the data prior to interpolation.

ACKNOWLEDGEMENTS

We would like to thank KAUST and the members of the University of Utah Tomography and Modeling/Migration (UTAM) Consortium (http://csim.kaust.edu.sa). We would like to thank S. Brown for his assistance with the up- and downgoing separation and C. Boonyasiriwat for revising the manuscript. We would like to thank Landmark for the University Software Grant and permission to use ProMax.

REFERENCES

Abma R. and Kabir N. 2005. Comparisons of interpolation methods. *The Leading Edge* **24**, 984–989.

Abma R. and Kabir N. 2006. 3D interpolation of irregular data with a POCS algorithm. *Geophysics* **71**, E91–E97.

Aoki N. 2009. Fast least-squares migration with a deblurring filter. *PhD thesis*, University of Utah, Utah, USA, 77 P.

Baumstein A., Hadidi M.T., Hinkley L. and Ross W.S. 2005. A practical procedure for application of 3D SRME to conventional marine data. *The Leading Edge* **24**, 254–258.

Berkhout A.J. and Verschuur D.J. 2006. Imaging of multiples reflections. *Geophysics* **71**, S1209–S1220.

Cao W. and Schuster G.T. 2010. Antialiasing condition and filter for the reciprocity equation of correlation type. *Geophysics* **75**, WB219–WB224.

Curry W. and Shan G. 2006. Interpolation of near offsets with multiples and prediction error filters. *EAGE Expanded Abstract*, G026.

Curry W. and Shan G. 2010. Interpolation of near offsets using multiples and prediction error filters. *Geophysics* **75**, WB153–WB164.

van Dedem E.J. and Verschuur D.J. 2005. 3D surface related multiple prediction: A sparse inversion approach. *Geophysics* **70**, V31–V43.

Dong S. and Schuster G.T. 2008. Interferometric extrapolation of OBS and SSP data. *SEG Expanded Abstracts*, 3013–3017.

Grion S., Exley R., Manin M., Miao X., Pica A., Wang Y. et al 2007. Mirror imaging of OBS data. *First Break* **25**, 37–42.

Groenestijn G.J.A and Verschuur D.J. 2009a. Estimating primaries by sparse inversion and application to near-offset data reconstruction. *Geophysics* **74**, A23–A28.

Groenestijn G.J.A and Verschuur D.J. 2009b. Estimating primaries and near-offset reconstruction by sparse inversion: Marine data application. *Geophysics* **74**, R119–R128.

Gulunay N. 2003. Seismic trace interpolation in the Fourier transform domain. *Geophysics* **68**, 355–369.
Hanafy Sh.M., Cao W. and Schuster G.T. 2009. Interferometric interpolation of 3D SSP data. *SEG Expanded Abstracts*, 3138–3142.
Huo S. and Wang Y. 2009. Improving adaptive subtraction in seismic multiple attenuation. *Geophysics* **74**, V59–V67.
Jiang Z., Yu J., and Schuster G.T. 2005. Migration of multiples. *The Leading Edge* **24**, 315–318.
Muijs R., Robertsson J.O.A. and Holliger K. 2007. Prestack depth migration of primary and surface-related multiple reflections: Part 1 - Imaging. *Geophysics* **72**, S59–S69.
Naghizadeh M. and Innanen K.A. 2011. Seismic data interpolation using a fast generalized Fourier transform. *Geophysics* **76**, V1–V10.
Ramirez A.C., Hokstad K. and Otnes E. 2007. Data-driven regularization/extrapolation using interferometry with the direct wave. *EAGE Expanded abstract*, B032.
Ramirez A.C. and Weglein A.B. 2009. Green's theorem as a comprehensive framework for data reconstruction, regularization, wavefield separation, seismic interferometry, and wavelet estimation: A tutorial. *Geophysics* **74** , W35–W62.
Schuster G.T. 2009. *Seismic Interferometry*. Cambridge Press, ISBN 978-0-521-87124-2.
Sheng J. 2001. Migrating multiples and primaries in CDP data by crosscorrelogram migration. *SEG Expanded Abstract*, 1297–1300.
Snieder R., Wapenaar K. and Larner K. 2006. Spurious multiples in interferometric imaging of primaries. *Geophysics* **71**, SI65–SI78.
Verschuur D. 2006. *Seismic Multiples Removal Technique*. *EAGE Publications*, Amsterdam.
Wang T. 2003. Multiple subtraction using an expanded multichannel matching filter. *Geophysics* **68**, 346–354.
Wang Y., Luo Y. and Schuster G.T. 2009. Interferometric interpolation of missing seismic data. *Geophysics* **74**, S137–S145.
Wapenaar K. and Fokkema J. 2006. Green's function representations for seismic interferometry. *Geophysics* **71**, S133–S146.
Zwartjes P.M. and Sacchi M.D. 2007. Fourier reconstruction of nonuniformly sampled, aliased seismic data. *Geophysics* **72**, V21–V32.

APPENDIX A

Acoustic reciprocity equation of correlation type with two states

Consider two states, one is the acoustic field associated with the multi-layered model shown in Fig. 1, where $G(\mathbf{x}|\mathbf{A})$ is interpreted as the acoustic wavefield excited by an interior harmonic point source at **A** and recorded at **x** and the other state is the acoustic field in the sea-floor model, which only consists in a water layer, a free surface and a sea floor, below which lies a homogeneous medium with the velocity and density of the second layer shown in Fig. 1. The Green's function associated with this state is defined as $G_0(\mathbf{x}|\mathbf{B})$ and does not contain reflections from any interfaces below the sea floor. The Helmholtz equations satisfied by these two Green's functions are

$$(\nabla^2 + k^2)G(\mathbf{x}|\mathbf{A}) = -\delta(\mathbf{x} - \mathbf{A}), \tag{A1}$$

$$(\nabla^2 + k_0^2)G_0(\mathbf{x}|\mathbf{B}) = -\delta(\mathbf{x} - \mathbf{B}), \tag{A2}$$

where $k = \omega/v(\mathbf{x})$ for the multi-layered model and $k_0 = \omega/v_0(\mathbf{x})$ for the sea-floor model. Applying the complex conjugate to both sides of equation (A2) gives

$$(\nabla^2 + k_0^2)G_0(\mathbf{x}|\mathbf{B})^* = -\delta(\mathbf{x} - \mathbf{B}). \tag{A3}$$

Multiplying both sides of equation (A1) with $G_0(\mathbf{x}|\mathbf{B})^*$ and both sides of equation (A3) with $G(\mathbf{x}|\mathbf{A})$ and subtracting the resulting two equations gives

$$\begin{aligned} &G(\mathbf{x}|\mathbf{A})\delta(\mathbf{x} - \mathbf{B}) - G_0(\mathbf{x}|\mathbf{B})^*\delta(\mathbf{x} - \mathbf{A}) \\ &= G_0(\mathbf{x}|\mathbf{B})^*(\nabla^2 + k^2)G(\mathbf{x}|\mathbf{A}) - G(\mathbf{x}|\mathbf{A})(\nabla^2 + k_0^2)G_0(\mathbf{x}|\mathbf{B})^*, \\ &= G_0(\mathbf{x}|\mathbf{B})^*\nabla^2 G(\mathbf{x}|\mathbf{A}) - G(\mathbf{x}|\mathbf{A})\nabla^2 G_0(\mathbf{x}|\mathbf{B})^* \\ &+ (k^2 - k_0^2)G_0(\mathbf{x}|\mathbf{B})^* G(\mathbf{x}|\mathbf{A}). \end{aligned} \tag{A4}$$

Applying the following identities

$$\begin{aligned} G_0(\mathbf{x}|\mathbf{B})^*\nabla^2 G(\mathbf{x}|\mathbf{A}) &= \nabla \cdot [G_0(\mathbf{x}|\mathbf{B})^*\nabla G(\mathbf{x}|\mathbf{A})] \\ &\quad -\nabla G_0(\mathbf{x}|\mathbf{B})^* \cdot \nabla G(\mathbf{x}|\mathbf{A}), \\ G(\mathbf{x}|\mathbf{A})\nabla^2 G_0(\mathbf{x}|\mathbf{B})^* &= \nabla \cdot [G(\mathbf{x}|\mathbf{A})\nabla G_0(\mathbf{x}|\mathbf{B})^*] \\ &\quad -\nabla G(\mathbf{x}|\mathbf{A}) \cdot \nabla G_0(\mathbf{x}|\mathbf{B})^*, \end{aligned} \tag{A5}$$

to equation (A4), we have

$$\begin{aligned} G(\mathbf{x}|\mathbf{A})\delta(\mathbf{x} - \mathbf{B}) - G_0(\mathbf{A}|\mathbf{B})^*\delta(\mathbf{x}-\mathbf{A}) &= \nabla \cdot [G_0(\mathbf{x}|\mathbf{B})^*\nabla G(\mathbf{x}|\mathbf{A}) \\ -G(\mathbf{x}|\mathbf{A})\nabla G_0(\mathbf{x}|\mathbf{B})^*] &+ (k^2 - k_0^2)G_0(\mathbf{x}|\mathbf{B})^* G(\mathbf{x}|\mathbf{A}). \end{aligned} \tag{A6}$$

A volume integration is then applied to equation (A6), where V_0 is the region bounded by the dashed lines in Fig. 1. Instead of defining the integration volume over the entire multi-layered model, the volume is restricted to the sea-layer where both the sea-floor model and the multi-layer model are the same. In this case, $k = k_0$ and $(k^2 - k_0^2)G_0(\mathbf{x}|\mathbf{B})^* G(\mathbf{x}|\mathbf{A}) = 0$ and we arrive at the reciprocity equation of correlation type for two different states:

$$\begin{aligned} G(\mathbf{B}|\mathbf{A}) - G_0(\mathbf{A}|\mathbf{B})^* = \int_{S_s} [&G_0(\mathbf{x}|\mathbf{B})^* \frac{\partial G(\mathbf{x}|\mathbf{A})}{\partial n_x} \\ &-G(\mathbf{x}|\mathbf{A})\frac{\partial G_0(\mathbf{x}|\mathbf{B})^*}{\partial n_x}]d^2x, \end{aligned} \tag{A7}$$

where S_s is the integration boundary; here the receiver line should be slightly below the source line, while the integration along the free surface vanishes because both Green's functions are zero. The contributions from the vertical boundaries at

infinity to the left and right will be ignored because they do not contribute useful events in the interpolation. Equation (A7) is a reciprocity equation of correlation type for two different states, which can be used for the interpolation or extrapolation of traces (Dong and Schuster 2008).

APPENDIX B

Detailed steps for interferometric interpolation

Figure (B1) shows practical steps for interferometric interpolation. These steps are used to obtain the final results shown in this work.

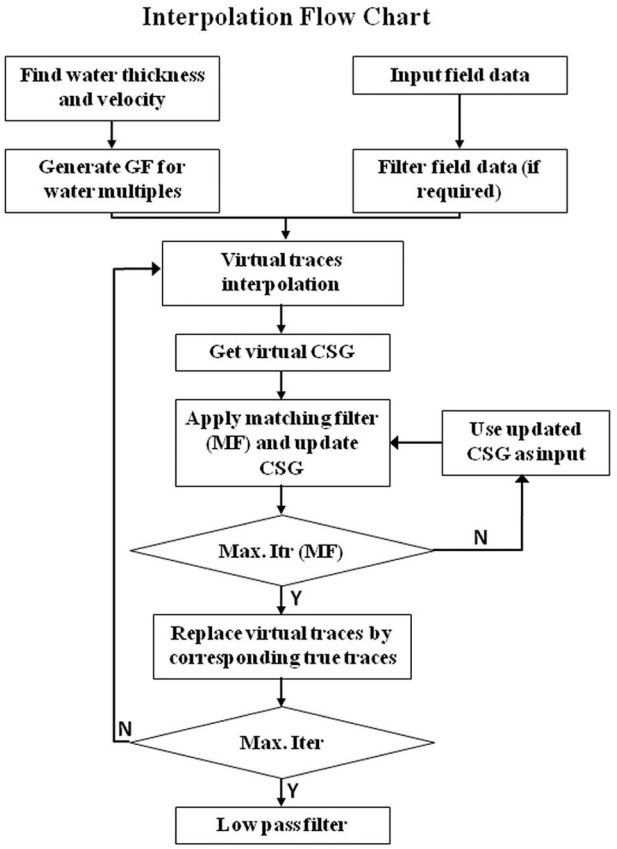

Figure B1 A flow chart showing the procedure for interferometric interpolation of marine seismic data. In case of using only upgoing field then only 1 iteration of interpolation and matching filter is required, while in the case of using the total field then more than 2 iterations of interpolation and matching filter are required.

- Field data should be low-pass filtered before starting the interferometric processing if high-frequency noise exists. The direct waves are removed because they do not contain information from below the sea floor and can cause artefacts in the interpolation procedures.
- The depth to the water bottom is either estimated from the data or obtained from a depth sounding survey. The velocity of the seismic waves in water can simply be found in the direct wave traveltimes picked from the field data.
- The depth to the water bottom and the acoustic velocity in water are used to generate the Green's function of the water layer in the two-layer model, where the first layer represents the water and the second layer corresponds to the layer just below the water layer. A ray-tracing method (for smooth water bottom) or finite-difference method (for complex water bottom) is used to generate the Green's function.
- The upgoing part of the field is recommended to be used in this approach, since it will produce fewer artefacts in the virtual shot gather and requires fewer iterations. However, the total field can also be used in this approach but we will need more iterations to obtain the final results.
- Data are interferometrically interpolated with equation (2) to fill in the missing traces.
- If the virtual shot gather from the previous step shows strong linear features, an FK filter can be used to remove them.
- A local matching filter is used to correct the virtual shot gather. The matching filter will be used only once in case of using upgoing field or will be iteratively repeated in the case of using the total field; here the input virtual shot gather for the (m^{th}) iteration step is the virtual shot gather that results from the ($m-1$) iteration.
- The virtual traces that coincide with true traces from the field data can be replaced by the true ones. This increases the accuracy of the virtual shot gather.
- The interferometric interpolation procedure can now be repeated using the virtual shot gather obtained from the previous step, this is only in case of using the total field.
- Finally, a low-pass filter is used to remove the high-frequency noise generated during these processing steps.